AGU PUBLICATIONS

JGR

Journal of Geophysical Research: Oceans

RESEARCH ARTICLE

10.1002/2016JC012399

Key Points:
- The turbulent fluxes through air-sea interface including momentum, sensible heat, and water vapor are systematically observed and analyzed
- CDN, CHN, and CEN decrease when wind speed less than 5 m/s. CDN keeps constant then increases with wind speed. CHN and CEN remain constant
- A new parameterization model is proposed as a function of Richardson number, which is free of the MOST and self-correlation

Correspondence to:
D. Zhao,
dlzhao@ouc.edu.cn

Citation:
Zou, Z., D. Zhao, B. Liu, J. A Zhang, and J. Huang (2017), Observation-based parameterization of air-sea fluxes in terms of wind speed and atmospheric stability under low-to-moderate wind conditions, *J. Geophys. Res. Oceans*, *122*, 4123–4142, doi:10.1002/2016JC012399.

Received 29 SEP 2016
Accepted 26 MAR 2017
Accepted article online 31 MAR 2017
Published online 18 MAY 2017

Observation-based parameterization of air-sea fluxes in terms of wind speed and atmospheric stability under low-to-moderate wind conditions

Zhongshui Zou[1], Dongliang Zhao[1], Bin Liu[2], Jun A Zhang[3,4], and Jian Huang[5]

[1]Physical Oceanography Institute, College of Oceanic and Atmospheric Sciences, Ocean University of China, Qingdao, China, [2]Environmental Modeling Center, National Centers for Environmental Prediction, National Weather Service, National Oceanic and Atmospheric Administration, College Park, Maryland, USA, [3]Hurricane Research Division, Atlantic Oceanographic and Meteorological Laboratory, National Oceanic and Atmospheric Administration, Miami, Florida, USA, [4]Cooperative Institute for Marine and Atmospheric Studies, University of Miami, Miami, Florida, USA, [5]Institute of Tropical and Marine Meteorology, China Meteorology Administration, Guangzhou, China

Abstract This study explores the behavior of the exchange coefficients for wind stress (C_D), sensible heat flux (C_H), and water vapor flux (C_E) as functions of surface wind speed (U_{10}) and atmospheric stability using direct turbulent flux measurements obtained from a platform equipped with fast-response turbulence sensors in a low-to-moderate wind region. Turbulent fluxes are calculated using the eddy-correlation method with extensive observations. The total numbers of quality-controlled 30 min flux runs are 12,240, 5813, and 5637 for estimation of C_D, C_H, and C_E, respectively. When adjusted to neutral stability using the Monin-Obukhov similarity theory (MOST), we found that C_{DN}, C_{HN}, and C_{EN} decrease with neutral-adjusted wind speed when wind speed is less than 5 m/s. C_{DN} is constant over the range 5 m/s $< U_{10N} <$ 12 m/s, then increases with U_{10N} when $U_{10N} >$ 12 m/s. In contrast, C_{HN} and C_{EN} exhibit no clear dependence on wind speed and are generally constant, with mean values of 0.96×10^{-3} and 1.2×10^{-3}, respectively. This behavior of neutral exchange coefficients is consistent with the findings of previous studies. We also found that C_{DN} under offshore winds is generally greater than that under onshore wind conditions, which is ascribed to the younger wind waves present due to the shorter fetch in the former case. However, this behavior is not exhibited by C_{HN} or C_{EN}. The original C_D, C_H, and C_E values without MOST adjustment are also investigated to develop a new parameterization based on wind speed and stability. Three stability parameters are tested, including the bulk Richardson number, stability as defined in COARE 3.0, and a simplified Richardson number using the Charnock parameter. This new parameterization is free of MOST and the associated self-correlation. Compared with previous studies and COARE 3.0 results, the new parameterization using the simplified Richardson number performs well, with an increased correlation coefficient and reduction of root-mean-square error and bias.

1. Introduction

In the atmospheric surface layer, the fluxes of momentum, heat, and water vapor between the atmosphere and ocean can be determined using the eddy-correlation method. These fluxes are defined as

$$\tau = -\rho\overline{u'w'} \tag{1}$$

$$Q_H = -\rho c_p \overline{w'\theta'} \tag{2}$$

$$E = -\rho\overline{w'q'} \tag{3}$$

where τ, Q_H, and E are the wind stress, sensible heat, and water vapor fluxes, respectively; ρ is air density; and c_p is the specific heat of air at constant pressure. u', w', θ', and q' are the fluctuations of horizontal wind velocity, vertical wind velocity, potential temperature, and specific humidity, respectively. The overbar indicates a time-averaged process. In practice, however, oceanographers and meteorologists often rely on bulk methods due to the scarcity of turbulence data [e.g., *Smith*, 1980; *Large and Pond*, 1982; *Fairall et al.*, 2003; *Drennan et al.*, 2007]. Air-sea fluxes can be estimated by

$$\tau = \rho C_D U^2 \quad (4)$$

$$Q_H = \rho c_p C_H U(\theta - \theta_0) \quad (5)$$

$$E = \rho C_E U(q - q_0) \quad (6)$$

where C_D, C_H, and C_E are the exchange coefficients of the momentum, heat, and water vapor fluxes, respectively. U, θ, and q are the mean values of wind speed, potential temperature, and specific humidity at a particular reference height above the sea surface, respectively. θ_0 is the surface temperature, and q_0 is the saturated specific humidity at the sea surface with the effect of salinity taken into account [*Fairall et al*., 1996]. Given the values of the exchange coefficients C_D, C_H, and C_E as well as sea surface temperature and humidity, wind speed, air temperature, and humidity at a reference height, estimates of wind stress and the fluxes of sensible heat and moisture in the atmospheric surface layer can be obtained using equations (4)–(6).

Many studies have shown that exchange coefficients depend on atmospheric stability and the height above the sea surface. To compare exchange coefficients obtained under differing conditions, the measured exchange coefficients C_D, C_H, and C_E are usually converted to the neutral exchange coefficients C_{DN}, C_{HN}, and C_{EN} at a height of 10 m based on the Monin-Obukhov similarity theory (MOST) [*Monin and Yaglom*, 1971].

MOST and the Charnock relationship [*Charnock*, 1955] are the basis of a large fraction of the air-sea bulk flux models embedded in general circulation and mesoscale models in use today. Despite its widespread usage and apparent overall success, physical interpretation of MOST can be ambiguous due to self-correlation and circular dependences [*Vickers et al*., 2015]. MOST employs an iterative process to predict turbulent fluxes in terms of exchange coefficients that depends on stability functions and thus on the turbulent fluxes of heat, moisture, and momentum through the Obukhov length L.

Based on the state-of-the-art Coupled Ocean-Atmosphere Response Experiment (COARE) bulk algorithm version 3.0 [*Fairall et al*., 2003; *Kara et al*., 2005] derived exchange coefficients that can be expressed as simple polynomial functions of wind speed and stability, which are parameterized by the air-sea temperature difference and relative humidity at the sea surface. This method implicitly depends on MOST due to its use of COARE 3.0. Using aircraft-based eddy-correlation measurements, *Vickers et al*. [2015] developed a formula for friction velocity that depends on wind speed and stability without use of MOST, the Obukhov length, or the Charnock relationship.

In this study, observational data obtained from a platform in the South China Sea between September 2010 and August 2012 were used to determine turbulent fluxes directly. Surface exchange coefficients were derived in two different ways, with and without MOST. The objective of this paper is to evaluate methods used in previous studies to derive exchange coefficients. We aim to develop a new parameterization of exchange coefficients in the region we studied.

2. Observational Data

The Flux Observation Platform in the South China Sea (FOPSCS) campaign was conducted on a platform operated jointly by the Guangzhou Institute of Tropical and Marine Meteorology and the China Meteorology Administration. The aim of FOPSCS was to study the mechanism of exchange in turbulent fluxes through the air-sea interface and to obtain accurate parameterizations of the exchange coefficients for momentum, heat, moisture, and carbon dioxide based on long-term observation. The location of the platform is 21°26.5′N, 111°23.5′E in the northern South China Sea. The shortest distance between the platform and the coastline is approximately 6.5 km, and the water depth is about 14 m (Figure 1).

An eddy-correlation system and wind monitors at five heights were installed on the platform to observe wind speed, temperature, and water vapor concentration. A three-dimensional ultrasonic anemometer deployed 20 m above the sea surface was used to measure wind velocity and sonic temperature at a frequency of 10 Hz. At the same height, an open-path CO_2/H_2O analyzer was used to observe water vapor concentrations with a sampling frequency of 10 Hz, and an infrared radiometer was used to observe the sea surface skin temperature every 30 min. A temperature and relative humidity probe was installed 20 m above mean sea level to record temperature and specific humidity as 10 min averages. Marine wind

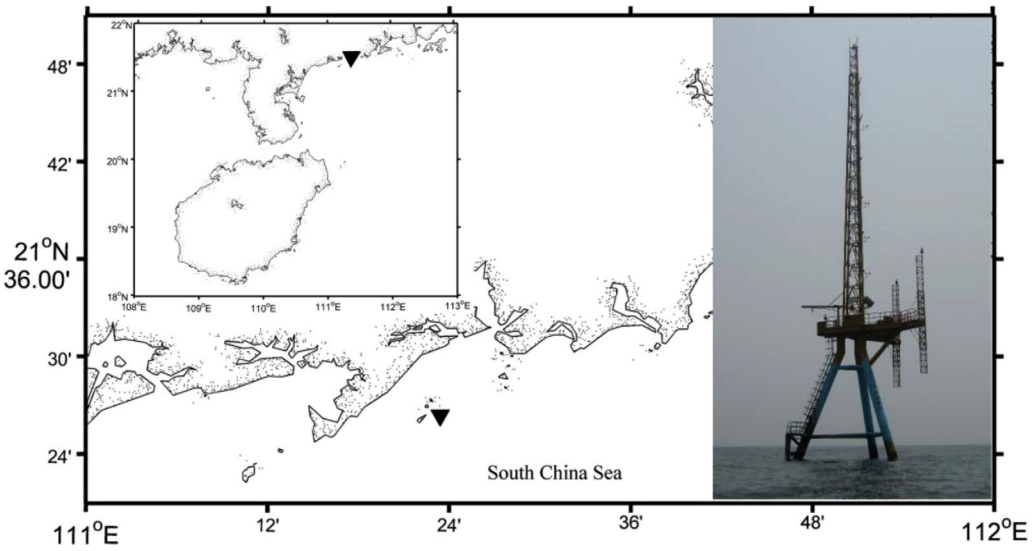

Figure 1. Maps and photograph of the platform; solid triangles denote the location of the platform on both maps.

monitors were mounted at 31.3, 23.4, 20.0, 16.4, and 13.4 m above mean sea level to measure wind speed and direction as 30 min averages. These observational data were collected using a CR 3000 Micrologger. Detailed information about the instruments used in this study can be found in Table 1.

3. Quality Control

In this study, the eddy-correlation method is used to calculate the momentum, heat, and water vapor fluxes. Before the estimation of fluxes, the raw observational data must be subjected to quality control procedures, including spike removal and tilt correction.

Spikes are typically characterized as short-duration and extraordinarily large-amplitude fluctuations, which are usually ascribed to brief electronic malfunctions or to contamination by rain droplets or other environmental factors. Following the method developed by *Vickers and Mahrt* [1997], any value more than 3.5 times the standard deviation is considered a spike. Data designated as spikes are removed from the time series and replaced by linear interpolations of the adjacent data. When four or more consecutive points have values that qualify as spikes, they are considered to be normal fluctuations rather than spikes. If a record contains more than 5% spikes, the entire record is discarded.

Large momentum flux deviations can be ascribed to the cross contamination of velocities that occurs in a tilted sonic anemometer, such that fluctuations in the longitudinal components of the wind appear as vertical velocity fluctuations, and vice versa [*Wilczak et al*., 2001]. On level terrain, the most straightforward solution is to be certain that turbulent wind sensors are installed exceptionally close to the true horizontal and vertical planes. However, over sloping or rough terrain, such as the sea surface, the most practical solution is to use a mean streamline coordinate system in which the x axis is parallel to the local mean wind direction and the z axis is orthogonal to x. Three methods for determining tilt angles relative to the mean

Table 1. Instruments Installed at the Platform During FOPSCS

Instrument	Model	Company	Parameters	Duration	Sample	Height
Ultrasonic Anemometer	CSAT3	Campbell S cientific, Inc.	Wind velocity Sonic virtual temperature	12 Sep 2010 to 8 Apr 2012	10 Hz	20.0 m
CO_2/H_2O Analyzer	LI-7500	LI-COR, Inc.	Moisture, CO_2, Pressure	12 Sep 2010 to 8 Apr 2012	10 Hz	20.0 m
Infrared radiometer	SI-111	Campbell, Inc.	Sea surface temperature	12 Sep 2010 to 28 Apr 2011	30 min (averaged)	20.0 m
Temperature and RH Probe	HMP45C	Campbell Scientific, Inc.	Air temperature, Relative humidity	12 Sep 2010 to 8 Apr 2012	10 min (averaged)	20.0 m
Wind monitor	05106	R.M. Young	Wind velocity	12 Sep 2010 to 28 Apr 2011	30 min (averaged)	31.3, 23.4, 20.0, 16.4, and 13.4 m

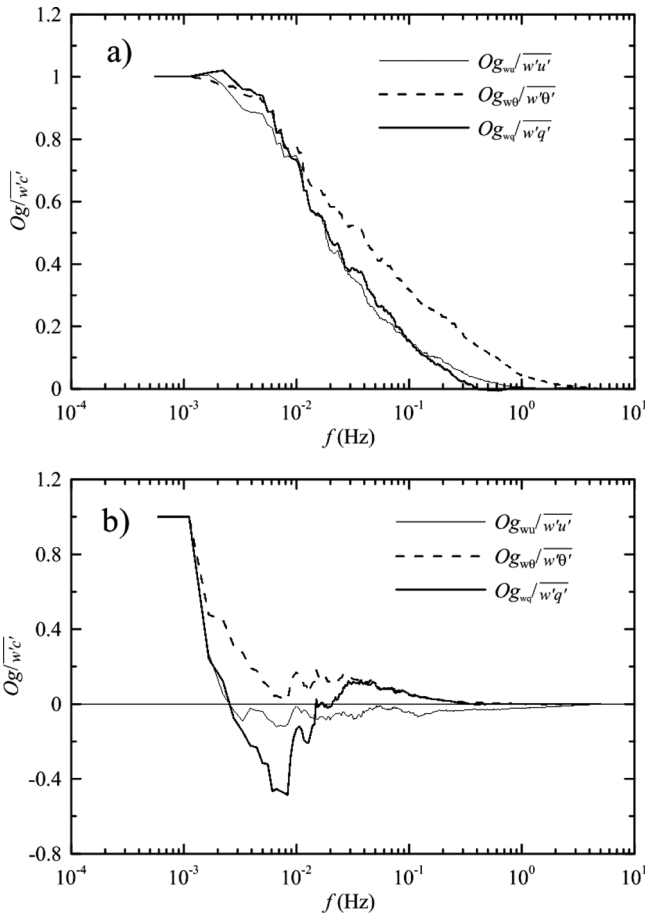

Figure 2. (a) Normalized ogives of turbulent fluxes as a function of frequency for a typical accepted flux run and (b) discarded flux run.

streamline coordinate system have been proposed. According to the work of *Wilczak et al*. [2001], the double rotation method that is most commonly used [*Tanner and Thurtell*, 1969] results in significant run-to-run stress errors due to sampling uncertainty of the mean vertical velocity. The triple rotation method [*McMillen*, 1988] results in even greater run-to-run stress errors due to the combined sampling errors of mean vertical velocity and crosswind stress. Compared to these two methods, the planar fit method is less susceptible to sampling errors and provides an unbiased estimate of lateral stress [*Wilczak et al*., 2001]. Therefore, the planar fit method of tilt correction is adopted in this study.

The turbulent fluxes through the air-sea interface are generally analyzed in the context of Reynolds averages, which are ensemble averages, in principle. In practice, they are usually replaced by time averages based on the ergodic hypothesis. Thus, choosing the time over which to average is necessary. Previous studies have usually used a fixed averaging time for all runs, typically from 15 to 60 min, regardless of stability, turbulence levels, or other factors [*Oncley et al*., 1996]. The cumulative or running integral of the cospectrum can be used to determine the frequency at which the covariance no longer changes. The reciprocal of this frequency is the minimum averaging time necessary to evaluate all flux contributions. The cumulative integral from high to low frequencies is called an ogive. We note that potential temperature, rather than sonic temperature, is used to calculate the sensible heat flux. The influences of cross-path (horizontal) wind speed and humidity are both considered in our estimates.

Figure 2 shows two examples of ogives normalized to the total covariance. If the normalized ogive increases monotonically with decreasing frequency and reaches 1.0, the corresponding run is utilized in further flux estimation (Figure 2a). Otherwise, the run is discarded (Figure 2b), as it might be contaminated by mesoscale motion in the atmosphere [*Vickers and Mahrt*, 2006; *French et al*., 2007; *Cook and Renfrew*, 2015]. Since most normalized ogives approach 1.0 at a frequency of 1.0×10^{-3} Hz, the averaging time should be greater than 17 min. To be consistent with the average winds measured by marine wind monitors, an averaging time of 30 min was chosen for this study, which is large enough to include all flux contributions. The ogives were calculated for each run in order to remove the influence of mesoscale motions.

4. Monin-Obukhov Similarity Theory

According to the Monin-Obukhov similarity theory (MOST), the following nondimensional profiles are valid for a surface layer that is horizontally homogeneous and stationary [*Monin and Yaglom*, 1971]

$$\frac{\kappa z}{u_*}\frac{\partial U}{\partial z} = \varphi_m\left(\frac{z}{L}\right) \tag{7}$$

$$\frac{\kappa z}{\theta_*}\frac{\partial \theta}{\partial z}=\varphi_h\left(\frac{z}{L}\right) \tag{8}$$

$$\frac{\kappa z}{q_*}\frac{\partial q}{\partial z}=\varphi_q\left(\frac{z}{L}\right) \tag{9}$$

where $\kappa = 0.4$ is the Von Kármán constant, z is height above the sea surface, $u_*=(-\overline{w'u'})^{1/2}$ is the friction velocity of air, $\theta_*=-\overline{w'\theta'}/u_*$ is the scaling temperature, $q_*=-\overline{w'q'}/u_*$ is the scaling specific humidity, $L=-u_*^3\theta_v/g\kappa\overline{w'\theta'_v}$ is the Obukhov length scale, θ_v is virtual temperature, $\overline{w'\theta'_v}$ is flux of virtual temperature (or buoyancy flux), and g is the acceleration due to gravity.

By integrating equations (7)–(9), the profiles of wind speed, potential temperature, and specific humidity can be expressed as

$$U(z)=(u_*/\kappa)[\ln(z/z_0)-\psi_m(z/L)] \tag{10}$$

$$\theta(z)-\theta_0=(\theta_*/\kappa)[\ln(z/z_{0h})-\psi_h(z/L)] \tag{11}$$

$$q(z)-q_0=(q_*/\kappa)\left[\ln(z/z_{0q})-\psi_q(z/L)\right] \tag{12}$$

where ψ_m, ψ_h, and ψ_q are stability functions and z_0, z_{0h}, and z_{0q} are the roughness lengths corresponding to the transport of momentum, heat, and moisture, respectively. Using equations (4)–(6), C_D, C_H, and C_E results in the theoretical, not just empirical, exchange coefficients, which can be expressed as [*Garratt*, 1992; *Andreas et al*., 2012]

$$C_D=\left[\frac{\kappa}{\ln(z/z_0)-\psi_m(z/L)}\right]^2 \tag{13}$$

$$C_H=\left[\frac{\kappa}{\ln(z/z_0)-\psi_m(z/L)}\right]\left[\frac{\kappa}{\ln(z/z_{0h})-\psi_h(z/L)}\right] \tag{14}$$

$$C_E=\left[\frac{\kappa}{\ln(z/z_0)-\psi_m(z/L)}\right]\left[\frac{\kappa}{\ln(z/z_{0q})-\psi_q(z/L)}\right] \tag{15}$$

Equations (13)–(15) show theoretically that exchange coefficients are related to atmospheric stability and the height of measurement. To compare measurements taken under various conditions, we usually eliminate the stability dependence and choose 10 m as a standard reference height. By doing so, equations (13)–(15) become the exchange coefficients for neutral stability, expressed as

$$C_{DN}=\left[\frac{\kappa}{\ln(10/z_0)}\right]^2 \tag{16}$$

$$C_{HN}=\frac{\kappa^2}{\ln(10/z_0)\ln(10/z_{0h})} \tag{17}$$

$$C_{EN}=\frac{\kappa^2}{\ln(10/z_0)\ln(10/z_{0q})} \tag{18}$$

The corresponding neutrally stable wind speed at 10 m is defined as [*Andreas et al*., 2012]

$$U_{10N}=U-(u_*/\kappa)\ln(z_0/10)+(u_*/\kappa)\psi_m \tag{19}$$

In practice, the Charnock relationship is usually applied to equations (16)–(18), where the roughness length z_0 is a function of u_*, and u_* is a function of the roughness length in equation (16). The roughness lengths for heat and moisture are functions of the Reynolds number [*Liu et al*., 1979]. Such a feedback loop can lead to extremely small estimates of the roughness length and momentum flux [*Mahrt et al*., 2001; *Vickers et al*., 2015].

As noted above, the basic assumption of MOST is that the nondimensional wind, temperature, and humidity profiles, φ_m, φ_h, and φ_q, respectively, are universal functions of z/L (equations (7)–(9)). However, the detailed forms of these functions are not given by the theory and thus must be determined experimentally in the

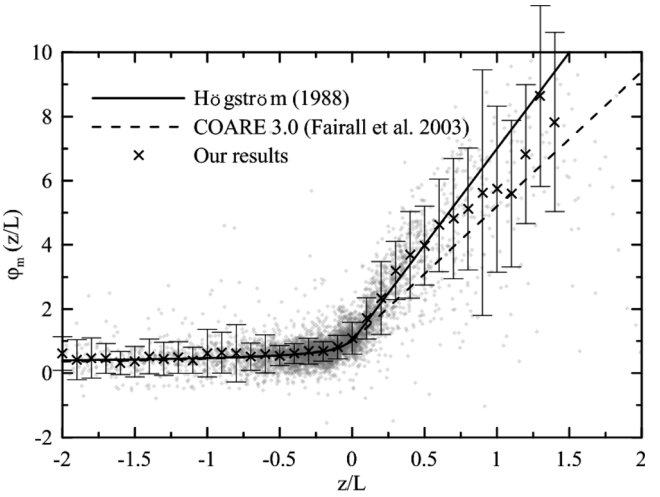

Figure 3. Plot of the universal function (φ_m) versus z/L. The individual flux runs from this study are denoted by gray dots. The mean values averaged for a bin size of 0.1 are denoted by black crosses. Error bars indicate ± 1 SD. Also shown are the curves from *Högström* [1988] and the COARE 3.0 algorithm [*Fairall et al.*, 2003].

field [*Högström*, 1996]. In the neutral condition, that is, for $z/L = 0$, these universal functions must equal a constant near unity. Compared with observational data, *Högström* [1996] indicated that various formulations of φ_m and φ_h are within 20% and 25% for $-0.02 \geq z/L \geq -2$, and 20% and 10% for $0.02 \leq z/L \leq 0.5$, respectively. For $z/L > 0.5$, the universal functions exhibit very large scatter, in which intermittent turbulence is common. Therefore, in practice, they are usually applied only to z/L values less than 2 [*Högström*, 1988 1996; *Klipp and Mahrt*, 2004].

In addition, the occurrence of u_* in both the Obukhov length and the nondimensional profiles may lead to considerable self-correlation. Self-correlation produces correlation of the same sign as that expected for stable conditions and can therefore lead to false confidence in MOST results [*Hicks* 1978; *Klipp and Mahrt*, 2004; *Baas et al.*, 2006].

Figure 3 shows φ_m using z/L calculated from our FOPSCS observational data, with error bars denoting ± 1 SD. The φ_m values of *Businger et al.* [1971] as modified by *Högström* [1988] and COARE 3.0 [*Fairall et al.*, 2003] are included for comparison. The two universal formulations and our observational data agree well under unstable conditions. However, considerable scattering occurs with increasing z/L under stable conditions, especially for large values of z/L. In the following analysis, data with more than 1 SD of scatter are discarded.

After these procedures, the total numbers of accepted 30 min runs were 12,240, 5813, and 5637 for the momentum, sensible heat, and moisture fluxes, respectively. These runs were used for further analysis.

5. Exchange Coefficients Under Neutral Conditions

5.1. C_{DN}

For several decades, studies have indicated that C_{DN} is a function of wind speed [*Smith*, 1980; *Wu*, 1980; *Large and Pond*, 1981; *Garratt*, 1977; *Geernaert et al.*, 1986; *Smith et al.*, 1992; *Edson et al.*, 2007; *Petersen and Renfrew*, 2009]. As shown in Figure 4, at very low wind speeds, motion near the sea surface is dominated by viscous flow, and the sea surface is aerodynamically smooth. With increasing wind speed, viscous flow is gradually depressed due to the enhancement of turbulent flow, which leads to reduction of C_{DN}. At wind speeds greater than 3–5 m/s, turbulent flow controls the air-sea momentum flux completely, and C_{DN} increases monotonically with wind speed. In recent years, some studies have suggested that C_{DN} is reduced or saturated at sufficiently high wind speeds, such as 30 m/s [*Powell et al.*, 2003; *Donelan et al.*, 2004; *Jarosz et al.*, 2007; *Holthuijsen et al.*, 2012]. The

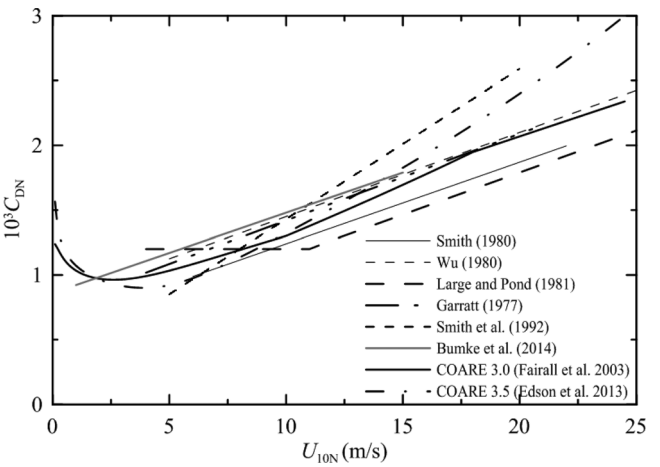

Figure 4. Several parameterizations of C_{DN} as a function of wind speed proposed in previous studies.

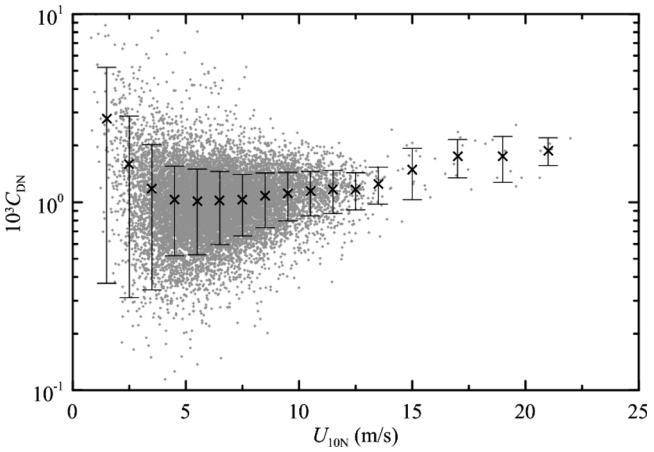

Figure 5. Original and bin-averaged 10 m neutral drag coefficient, C_{DN}, versus U_{10N}. For wind speeds below and above 13 m/s, the bin size is 1 m/s and 2 m/s, respectively. Crosses denote bin-averaged values and their error bars indicate ±1 SD.

maximum surface wind speed in our observational data set is < 20 m/s, which is not large enough to test for this saturation effect of C_D values at high wind speed.

Figure 5 shows the original data and bin-averaged 10 m neutral coefficient C_{DN} values against U_{10N} estimated from our observational data obtained through FOPSCS. For wind speeds below 13 m/s, a bin size of 1 m/s was chosen. For wind speeds above 13 m/s, a 2 m/s bin was used in order to include more data for mean estimation. Despite large scatter, the dominant features are similar to those found in earlier studies, such as an apparent local minimum in C_{DN} at a wind speed of about 5 m/s. Based on aircraft-based eddy-correlation measurements, *Vickers et al.* [2013] suggested that C_{DN} is very sensitive to the analysis method in weak wind conditions. Following *Vickers et al.* [2013], we investigate how sensitive C_{DN} is to the analysis method employed. The five bin-averaging methods (denoted 1–5) we investigated include

$$C_{DN1} = \left[(\overline{w'u'}^2 + \overline{w'v'}^2)^{1/2} U_{10N}^{-2} \right] \tag{20}$$

$$C_{DN2} = \left[(\overline{w'u'}^2 + \overline{w'v'}^2)^{1/2} \right] [U_{10N}]^{-2} \tag{21}$$

$$C_{DN3} = \left(\left[\overline{w'u'} \right]^2 + \left[\overline{w'v'} \right]^2 \right)^{1/2} [U_{10N}]^{-2} \tag{22}$$

$$C_{DN4} = \left[u_*^2 U_{10N}^{-2} \right] \tag{23}$$

$$C_{DN5} = \left[u_*^2 \right] \left[U_{10N}^{-2} \right] \tag{24}$$

where the square brackets denote U_{10N} bin averaging. These bin-averaging methods correspond to bin-averaged C_{DN} including the crosswind component (equation (20)), bin-averaged stress including the crosswind component (equation (21)), bin-averaged along-wind and crosswind components and U_{10N} (equation (22)), bin-averaged u_* and U_{10N} (equation (23)), and bin-averaged C_{DN} (equation (24)), respectively.

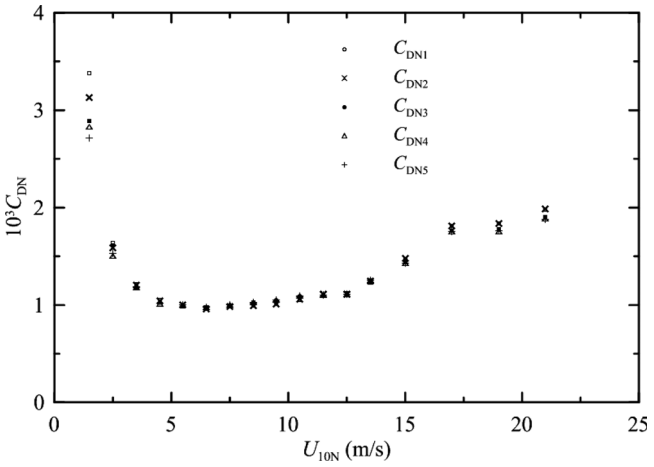

Figure 6. C_{DN} versus wind speed calculated by equations (20)–(24).

Figure 6 shows C_{DN} calculated using these five analysis methods. Distinct differences appear at a wind speed of 1 m/s. For wind speeds greater than 2 m/s, the five analysis methods are consistent, with a small reduction caused by excluding the crosswind component at wind speeds greater than 16 m/s. Our results are similar to those obtained by *Vickers et al.* [2013] (see their Figure 4). It is notable that distinct differences among analysis methods occur where the data are sparse. Therefore, we concluded that the neutral drag coefficient C_{DN} is not sensitive to differences among the various analysis methods expressed by

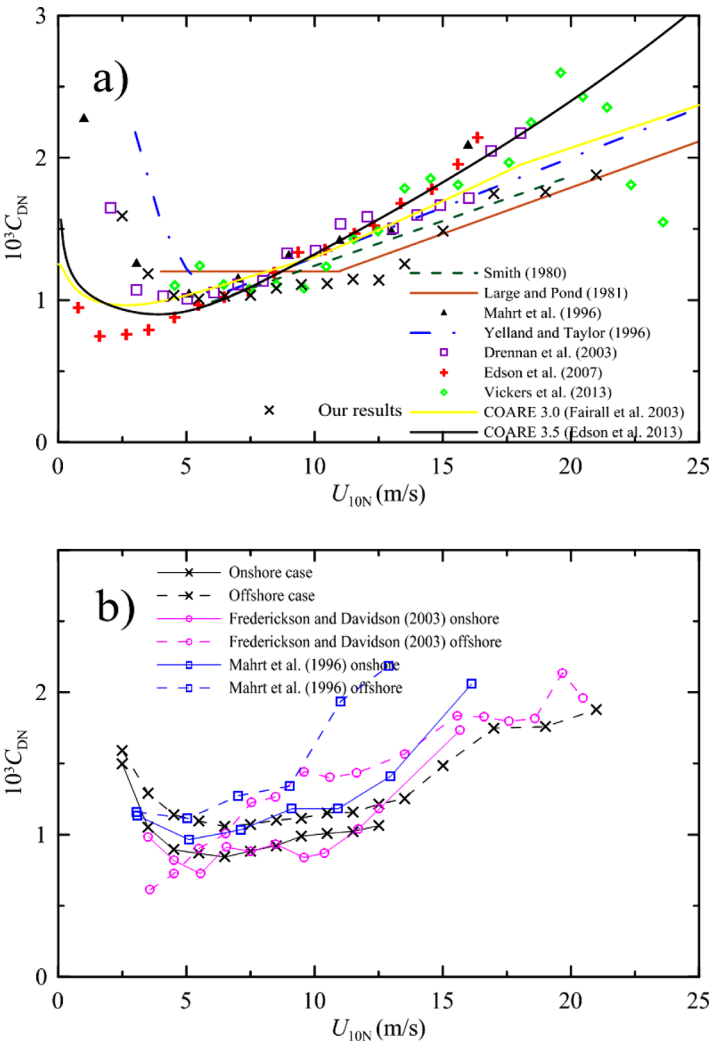

Figure 7. Drag coefficients versus wind speed. (a) Our results compared with previous studies including *Smith* [1980], *Large and Pond* [1981], *Mahrt et al*. [1996], *Yelland and Taylor* [1996], *Drennan et al*. [2003], *Edson et al*. [2003], COARE 3.0 [*Fairall et al*., 2003], COARE 3.5 [*Edson et al*., 2013], and *Vickers et al*. [2013]. (b) Comparison of offshore and onshore drag coefficients based on the observational data in this study, *Mahrt et al*. [1996], and *Frederickson and Davidson* [2003].

equations (21)–(24), and that the distinct differences at low wind speeds can be ascribed primarily to the small sample size.

For wind speeds below 5 m/s, C_{DN} decreases with wind speed, which agrees well with the findings of *Drennan et al*. [2003]. A minimum in the 10 m neutral value of the drag coefficient occurred at 5 m/s, between the 4 m/s suggested by *Vickers et al*. [2013] and 6 m/s by *Yelland and Taylor* [1996]. All observations are significantly greater than the estimates from COARE 3.0, which can be ascribed to aerodynamically smooth viscous flow. Also note that C_{DN} may be affected by ocean surface currents or momentum fluxes induced by swell at very low wind speeds [*Grachev and Fairall*, 2001]. For 5 m/s $< U_{10N} <$ 12 m/s, C_{DN} remains nearly constant with wind speed, with a value around 0.001. *Large and Pond* [1981] and *Vickers et al*. [2013] obtained similar results where C_{DN} was constant around 0.0013 and 0.0012 between 4 m/s and 10 m/s. For $U_{10N} > 12$ m/s, C_{DN} increases quickly with wind speed due to the limited fetch of offshore winds. Young wind waves contribute greatly to sea-surface roughness, as they break strongly. The C_{DN} saturation suggested by *Vickers et al*. [2013] was not evident in our observations.

Drag coefficients under offshore wind conditions are greater than those with onshore wind, which agrees with some previous studies [*Smith*, 1980; *Mahrt et al*., 1996; *Sun et al*., 2001]. A larger offshore drag coefficient is usually ascribed to younger, growing waves that cannot reach equilibrium with the prevailing wind field due to limited fetch. This fetch effect can be tested by separating drag coefficients into offshore and onshore cases based on wind direction. The results of such separation are shown in Figure 7b, along with observational data from *Mahrt et al*. [1996] and *Fredrickson and Davidson* [2003]. Similar to these previous studies, for a given wind speed, the drag coefficients of offshore winds are generally larger than those of onshore winds. It is clear that the fetches in the offshore cases are greater than those in the onshore cases. As noted by *Frederickson and Davidson* [2003], this observation is expected, as the wave field of short-fetch offshore winds cannot reach equilibrium with the prevailing wind field as quickly. These younger, growing waves have steeper slopes and present a rougher surface to the overlying atmosphere, resulting in higher drag coefficients. In the onshore case, wind waves come from the open ocean with a relatively long fetch, and thus the wave steepness is smaller, inducing smaller drag coefficients.

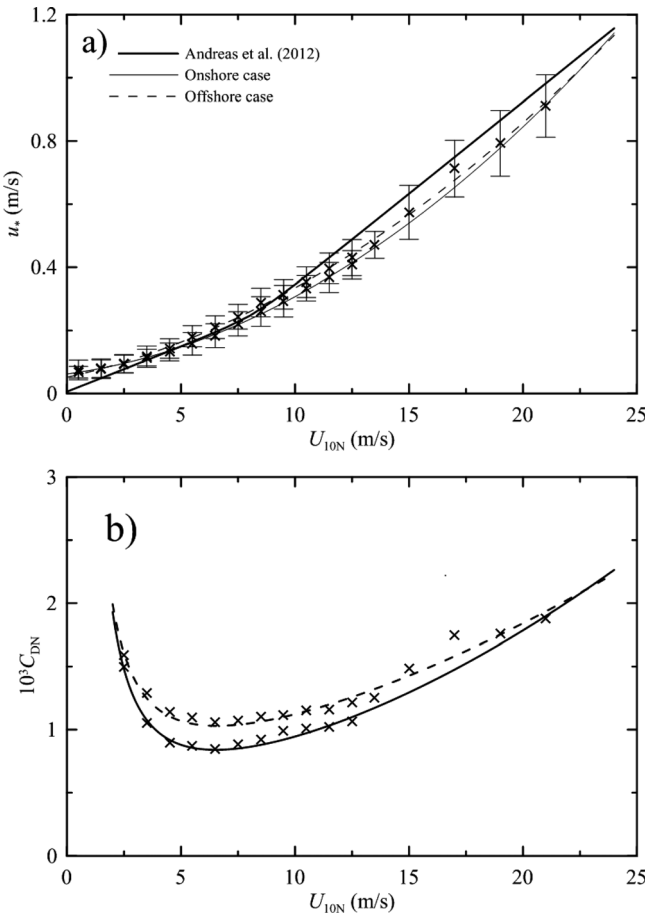

Figure 8. (a) The u_* versus U_{10N} relationship with the parameterizations of *Andreas et al.* [2012] and equation (25), and (b) the drag coefficient C_{DN} versus U_{10N} with the parameterization of equation (26).

Another factor that influences the drag coefficient in coastal regions is limited water depth. However, the effect of water depth on the drag coefficient seems to be ambiguous. It is generally accepted that drag coefficients in shallow water are greater than those in deep water. However, this behavior cannot be confirmed using the observational data shown in Figure 7a. Although the COARE 3.5 [*Edson et al.*, 2013] and *Yellan and Taylor* [1996] results were obtained from the open ocean (deep water), they do not exhibit a clear trend of being smaller than those of *Mahrt et al.* [1996, 4 m], *Edson et al.* [2007, 13 m], *Smith* [1980, 59 m], *Large and Pond* [1981, 59 m], and *Drennan et al.* [2003, 100 m] for shallow water. In the offshore wind case, the waves are so young that the effect of water depth can be neglected. In the onshore case, the reason for the lack of a water depth effect remains to be elucidated.

Figure 7a shows that there are three apparent wind speed regimes in our observational data, which agree well with the results of *Vickers et al.* [2013]. For comparison, the observational data from Figure 4 of *Drennan et al.* [2003] and Figure 5 of *Vickers et al.* [2013], as well as the calculations of *Smith* [1980], *Large and Pond* [1981], *Yelland and Taylor* [1996], COARE 3.0 [*Fairall et al.*, 2003], and COARE 3.5 [*Edson et al.*, 2007], are also presented in Figure 7a.

From the definition of C_{DN}, it is reasonable to infer that u_* is proportional to U_{10N} with a proportionality constant of $(C_{DN})^{1/2}$. Recently, *Foreman and Emeis* [2010] and *Andreas et al.* [2012] suggested that u_* is related linearly to U_{10N}, not proportionally. Figure 8a shows u_* as a function of U_{10N} from our observational data. It is clear that u_* is not related linearly to U_{10N}. Using the least squares method, their relationship can be parameterized in the offshore and onshore cases,

$$u_* = \begin{cases} 0.0015U_{10N}^2 + 0.0099U_{10N} + 0.062, & \text{for onshore wind} \\ 0.0012U_{10N}^2 + 0.016U_{10N} + 0.052, & \text{for offshore wind} \end{cases} \tag{25}$$

The correlation coefficient is 0.99. Therefore, the neutral drag coefficients in the onshore and offshore cases can be expressed as

$$C_{DN} = \begin{cases} \left(0.0099 + 0.0015U_{10N} + 0.062U_{10N}^{-1}\right)^2, & \text{for onshore wind} \\ \left(0.016 + 0.0012U_{10N} + 0.052U_{10N}^{-1}\right)^2, & \text{for offshore wind} \end{cases} \tag{26}$$

Figure 8b compares calculated C_{DN} with the parameterization of equation (26). The benefit of equation (26) is that it does not require piecewise functions to include weak wind regimes, as does the method of *Yelland and Taylor* [1996], although it performs poorly between 17 and 22 m/s. As mentioned above, the results for this regime are somewhat uncertain due to sparse data.

Table 2. Previous Field Studies Measuring C_{HN} and C_{EN}

Authors	10^3C_{HN}	Range of U_{10N}	10^3C_{EN}	Range of U_{10N}
Pond et al. [1971]			1.2	$3.93 < U_{10N} < 7.22$
Large and Pond [1982]	1.13	$4 < U_{10N} < 25$	1.15	$4 < U_{10N} < 14$
Smith [1989]			1.2	$5 < U_{10N} < 18$
Bradley et al. [1991]	1.03	$4 < U_{10N} < 6$	0.89	$4 < U_{10N} < 6$
Decosmo et al. [1996]	1.1	$U_{10N} < 23$	1.1	$U_{10N} < 18$
Banner et al. [1999]	0.62–1.56	$2 < U_{10N} < 19$	0.77–1.09	$2 < U_{10N} < 19$
McGillis et al. [2004]			0.8–3.0	$U_{10N} < 12$
Drennan et al. [2007]			1.18	$U_{10N} < 30$
Zhang et al. [2008]	1.16	$15 < U_{10N} < 30$	1.16	$15 < U_{10N} < 30$
Petersen and Renfrew [2009]	1.63	$15 < U_{10N} < 19$	1.57	$15 < U_{10N} < 19$
Bumke et al. [2014]	$1.03 + 0.012U_{10N}$	$U_{10N} < 15$	$1.06 + 0.005U_{10N}$	$U_{10N} < 15$
Cook and Renfrew [2015]	0.92–1.36	$6 < U_{10N} < 24$	0.83–1.77	$6 < U_{10N} < 24$

5.2. C_{HN} and C_{EN}

Compared with drag coefficients, the exchange coefficients of heat and water vapor flux are rarely reported due to the lack of real-time measurement instruments suitable for the marine environment [*Drennan et al.*, 2007]. Table 2 lists previous observations of C_{HN} and C_{EN}. Unlike C_{DN}, most studies suggest that C_{HN} and C_{EN} do not depend on wind speed and are nearly constant with wind speed, with a range from 0.6 to 1.6 $\times$ 10^{-3}. Even under high wind conditions, where wave breaking and sea spray are believed to be important exchange processes, wind dependence is not evident [*Zhang et al.*, 2008; *Petersen and Renfrew*, 2009; *Cook and Renfrew*, 2015].

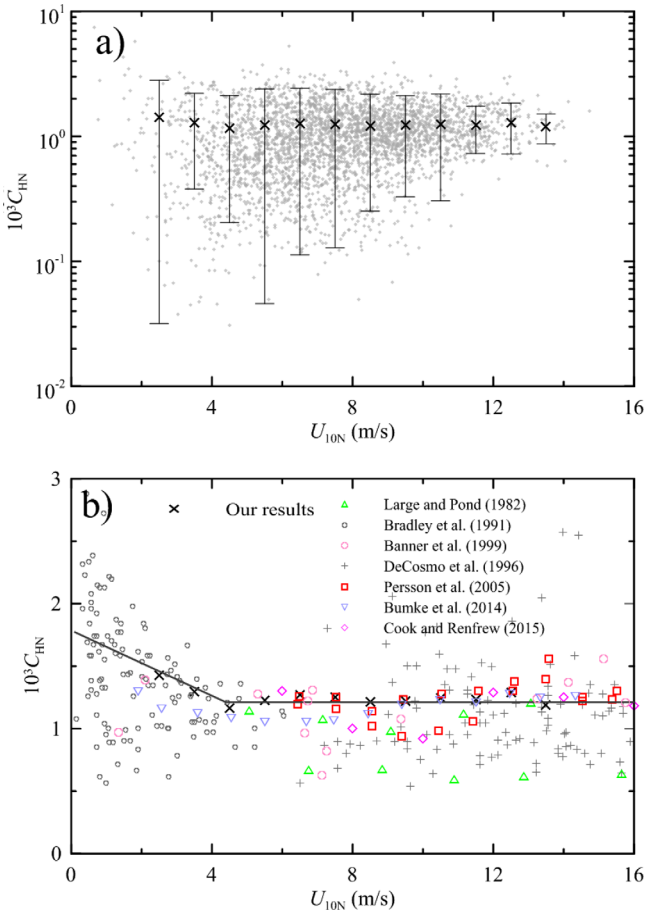

Figure 9. The neutral exchange coefficient C_{HN} versus wind speed U_{10N}: (a) our observational results (gray dots) and average values over 1 m/s bins (black crosses), error bars indicate $\pm$1 SD, and (b) comparison of our results with previous studies and equation (27), indicated by the solid line.

Figures 9 and 10 show the exchange coefficients of heat and water vapor flux against wind speed based on our observations and previous studies. Unlike the drag coefficient, these factors do not show a clear dependence on wind speed. The mean C_{HN} in our results varied between 1.17 $\times$ 10^{-3} and 1.42 $\times$ 10^{-3}, with an average value of 1.25 $\times$ 10^{-3}, and mean C_{EN} values range from 0.81 to 1.23 $\times$ 10^{-3} with an average of 0.97 $\times$ 10^{-3} for U_{10N} from 2 to 14 m/s. This is consistent with the results of *Large and Pond* [1982], HEXOS [*DeCosmo et al.*, 1996], FASTEX [*Persson et al.*, 2005], *Cook and Renfrew* [2015], and COARE 3.0. As with C_{DN}, we also separated the data into onshore and offshore cases for C_{HN} and C_{EN}. However, no significant differences were found (data not shown).

Upon close inspection of Figures 9 and 10, it is apparent that there is a weak reduction of both C_{HN} and C_{EN} with wind speed under weak wind conditions. The same behavior was observed by *Bradley et al.* [1991]. Using the least squares method, C_{HN} and C_{EN} can be parameterized as a stepwise function of wind speed

$$10^3 C_{HN} = \begin{cases} 1.72 - 0.13 U_{10N} & \text{for } U_{10N} < 4\,\text{m/s} \\ 1.20 & \text{for } U_{10N} \geq 4\,\text{m/s} \end{cases} \quad (27)$$

$$10^3 C_{EN} = \begin{cases} 1.44 - 0.12 U_{10N} & \text{for } U_{10N} < 4\,\text{m/s} \\ 0.96 & \text{for } U_{10N} \geq 4\,\text{m/s} \end{cases} \quad (28)$$

For comparison, Eq. (27) and Eq. (28) are plotted in Fig. 9 and Fig. 10, respectively.

6. Exchange Coefficients Versus Stability

As noted above, in order to compare exchange coefficients measured under different stability conditions, they are usually adjusted to neutral stability conditions using MOST. MOST requires an iterative process to predict the turbulent momentum and heat fluxes from exchange coefficients that depend on stability functions. In order to avoid this iterative process, some studies have tried to replace the stability correction with a term representing stability parameters, such as air-sea temperature difference, relative humidity (RH), or the comprehensive parameter, Richardson number [*Kara et al*., 2005; *Vickers et al*., 2015]. These studies suggest that the effects on turbulent fluxes must be taken into account when calculating exchange coefficients. The benefit of these algorithms is that they do not require iteration to account for stability, and thus they are computationally efficient, which is necessary for application in high-resolution coupled atmosphere-ocean circulation models.

Figure 11 shows the relationships between neutral exchange coefficients and stability parameters including the sea-air temperature difference $\Delta\theta = \theta_0 - \theta_{10}$, RH, and the sea-air specific humidity difference $\Delta q = q_0 - q_{10}$. The

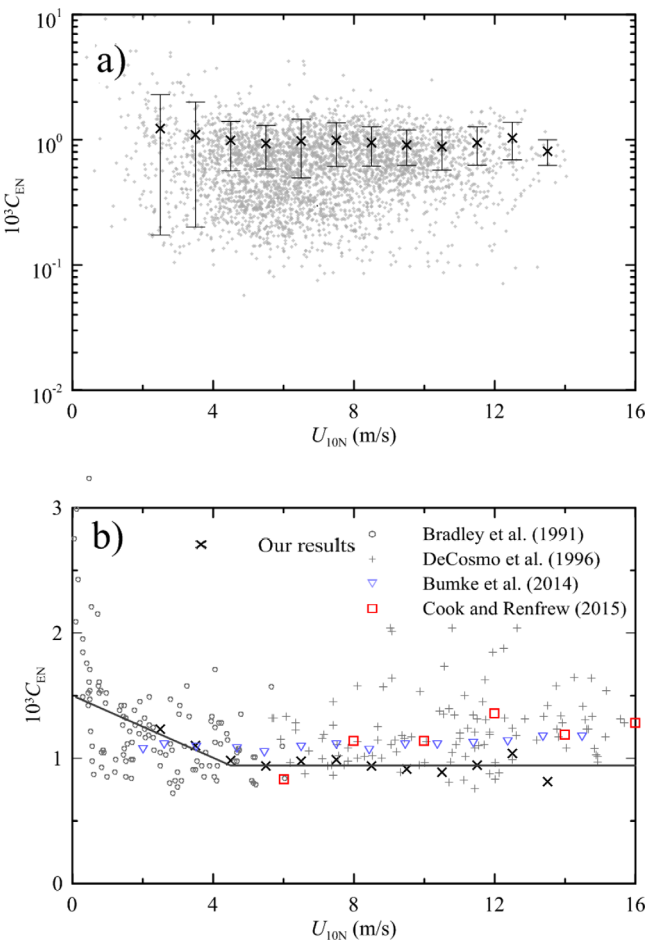

Figure 10. As described in Figure 9, but for C_E.

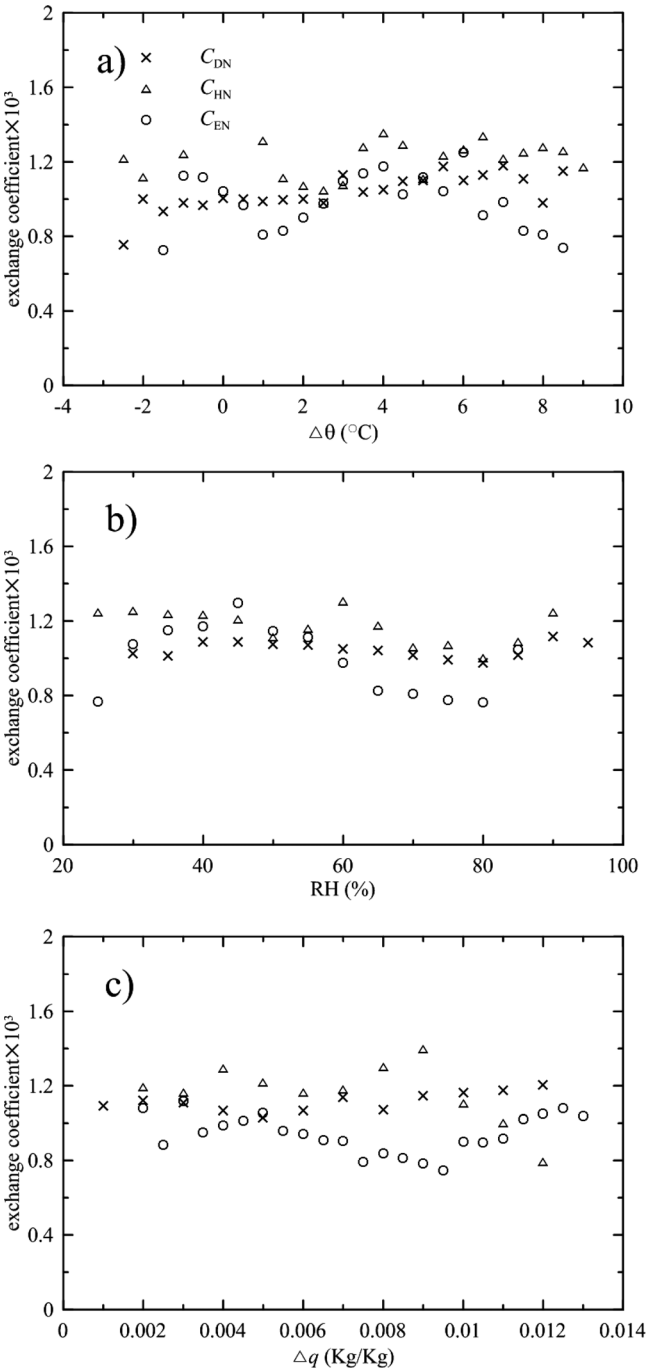

Figure 11. (a) Neutral exchange coefficients versus sea-air temperature difference, (b) relative humidity, and (c) sea-air specific humidity difference.

exchange coefficients do not show a clear trend with these stability parameters after stability correction using MOST, although there is large scatter.

Using the same format as in Figure 11, Figure 12 shows the exchange coefficients as a function of $\Delta\theta$, RH, and Δq. This figure indicates that the observed exchange coefficients increase with $\Delta\theta$, which means that turbulent mixing is enhanced under the unstable conditions induced by a large air-sea temperature difference (Figure 12a). This result is qualitatively consistent with *Kara et al*. [2005], while *Toffoli et al*. [2012] did not find a significant dependence on $\Delta\theta$. Increased humidity would be expected to decrease air density,

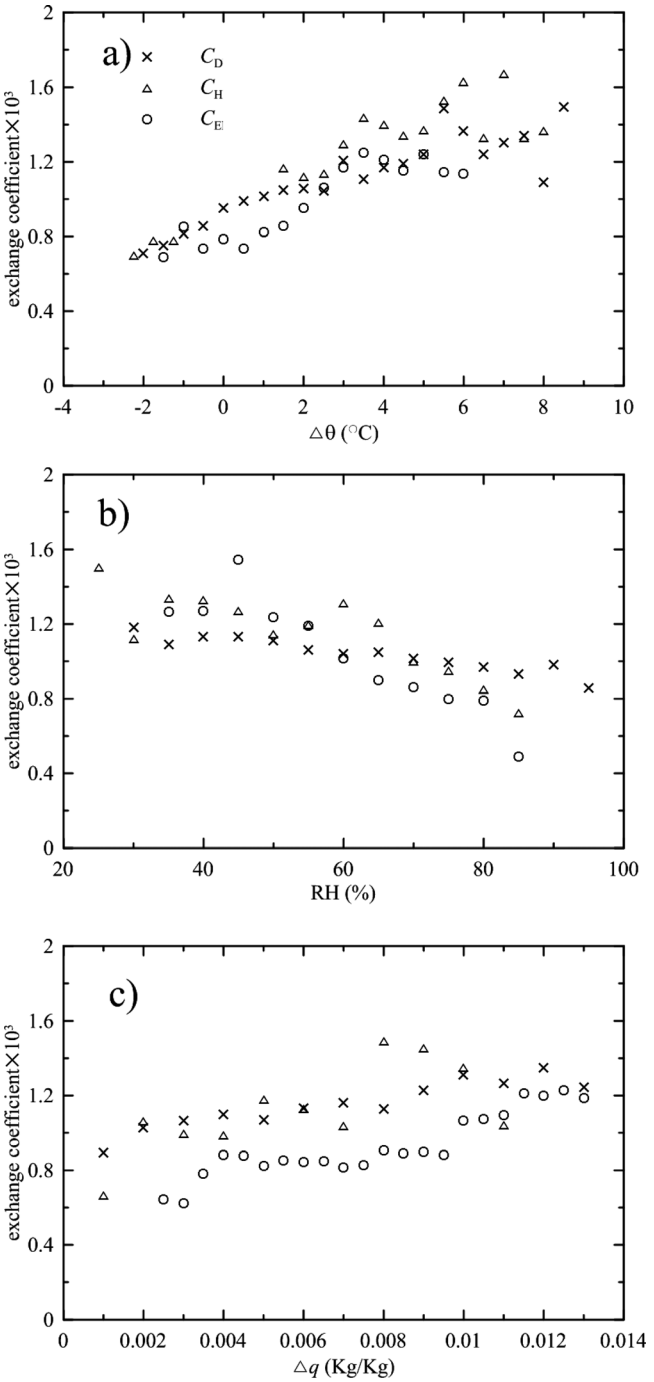

Figure 12. (a) Measured exchange coefficients without application of MOST versus sea-air temperature difference, (b) relative humidity, and (c) sea-air specific humidity difference.

increase buoyancy, and in turn increase friction velocity and drag coefficient [*Bianco et al.*, 2011]. However, the measured exchange coefficients show a surprising reduction with RH, consistent with the findings of *Kara et al.* [2005] and *Toffoli et al.* [2012] (Figure 12b). This feature is further confirmed by the increase in measured exchange coefficients with Δq, shown in Figure 12c.

To describe the dependences between the measured exchange coefficients and various stability parameters quantitatively, linear regressions were calculated. The results are displayed in Table 3.

Table 3. Linear Regressions Between the Measured Exchange Coefficients and Three Stability Parameters Including $\Delta\theta$, RH, and Δq, Where R Is the Correlation Coefficient

	$C_x = a + b\Delta\theta$			$C_x = a + b\mathrm{RH}$			$C_x = a + b\Delta q$		
	a	b	R	a	B	R	a	b	R
C_D	0.92	0.060	0.90	1.30	−0.0040	0.94	0.94	30.08	0.92
C_H	0.97	0.079	0.88	1.63	−0.009	0.84	0.84	48.02	0.69
C_E	0.82	0.0762	0.89	1.97	−0.017	0.91	0.55	48.75	0.90

7. New Parameterization of Exchange Coefficients

Owing to the limitations of MOST, some studies have parameterized the exchange coefficients with an explicit function of temperature and humidity to describe the stability contribution to turbulent fluxes [*Kara et al*., 2005]. Therefore, the exchange coefficient C_x can be expressed as

$$C_x = C_{xu}(U)G_x(R_0) \tag{29}$$

where $C_{xu}(U)$ and $G_x(R_0)$ represent the contributions of shear and buoyancy, respectively, and R_0 is a modified Richardson number describing stability. For simplicity, $C_{xu}(U)$ can be obtained by direct substitution of equations (26), (27), and (28) for momentum flux, sensible heat flux, and moisture flux, respectively. *Vickers et al*. [2015] defined R_0 as a bulk Richardson number

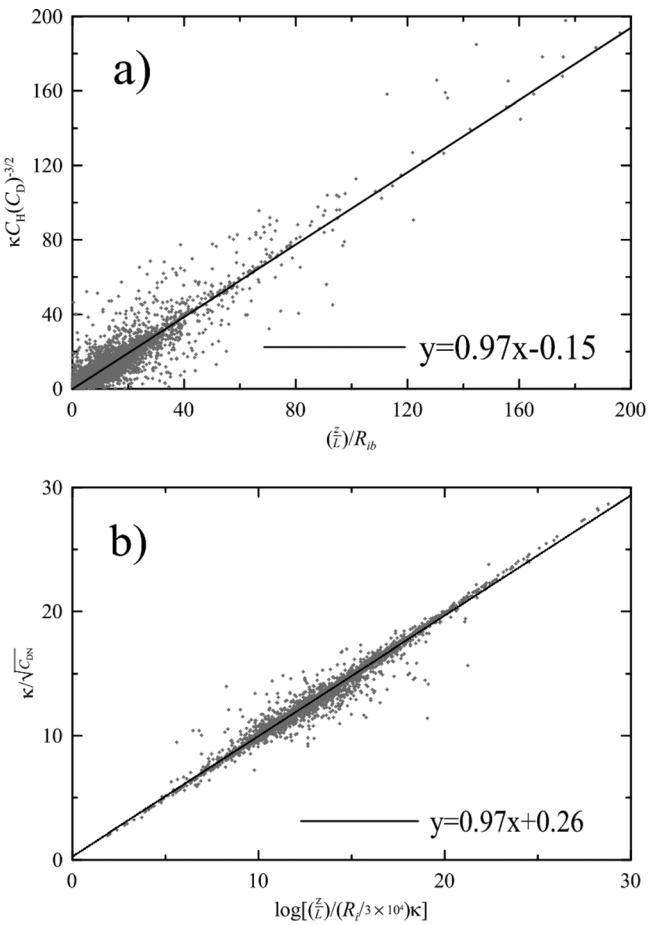

Figure 13. Comparison of equations (33) and (34) with our observations. The solid lines are best-fit lines. (a) z/L versus R_{ib}; (b) z/L versus R_i.

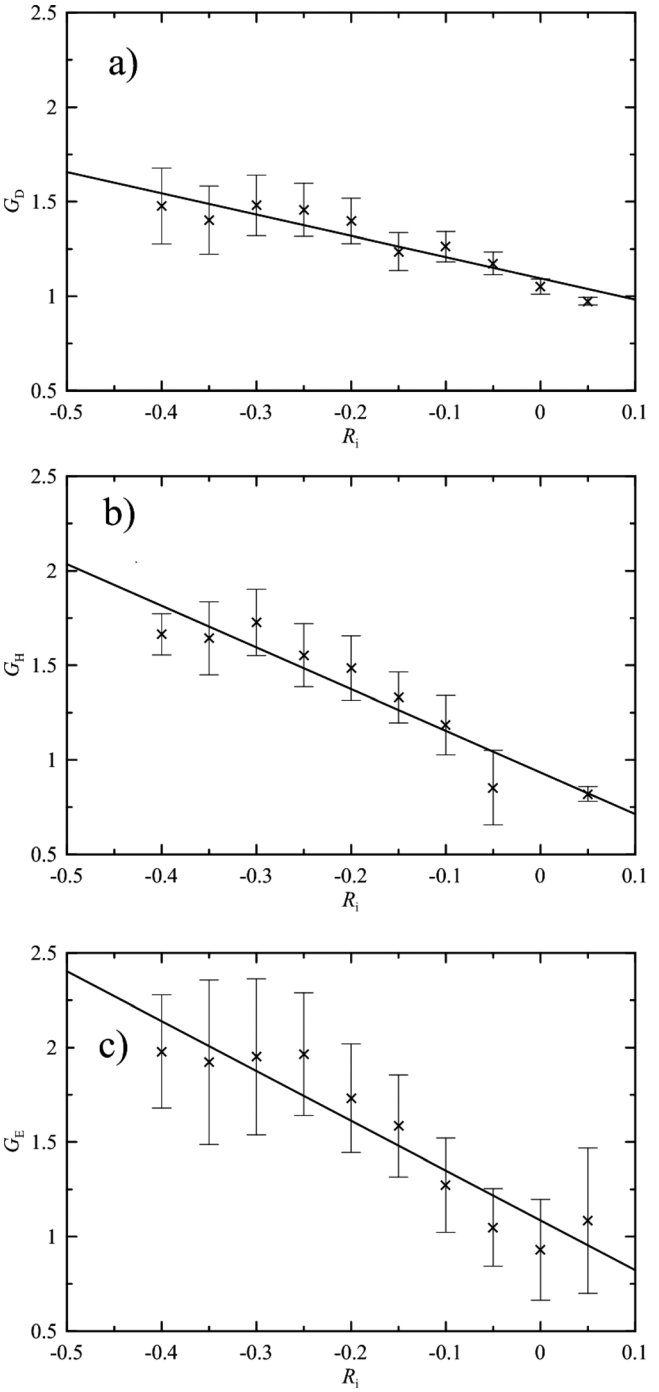

Figure 14. The stability function G_x versus R_i, for (a) G_D, (b) G_H, and (c) G_E.

$$R_{ib} = \frac{(\theta_v - \theta_{v0})gz}{\theta_v U^2} \tag{30}$$

where $\theta_v = \theta(1 + 0.61q)$ is the virtual potential temperature at height z and g is gravitational acceleration. R_{ib} describes the contributions of temperature, humidity, and wind speed to stability. It also strongly depends on the height of measurement, which limits its application. At the atmospheric boundary, u_*, θ_*, q_*, and z_0 are assumed to be constant with height. In place of R_{ib}, we substitute R_i, which is defined as

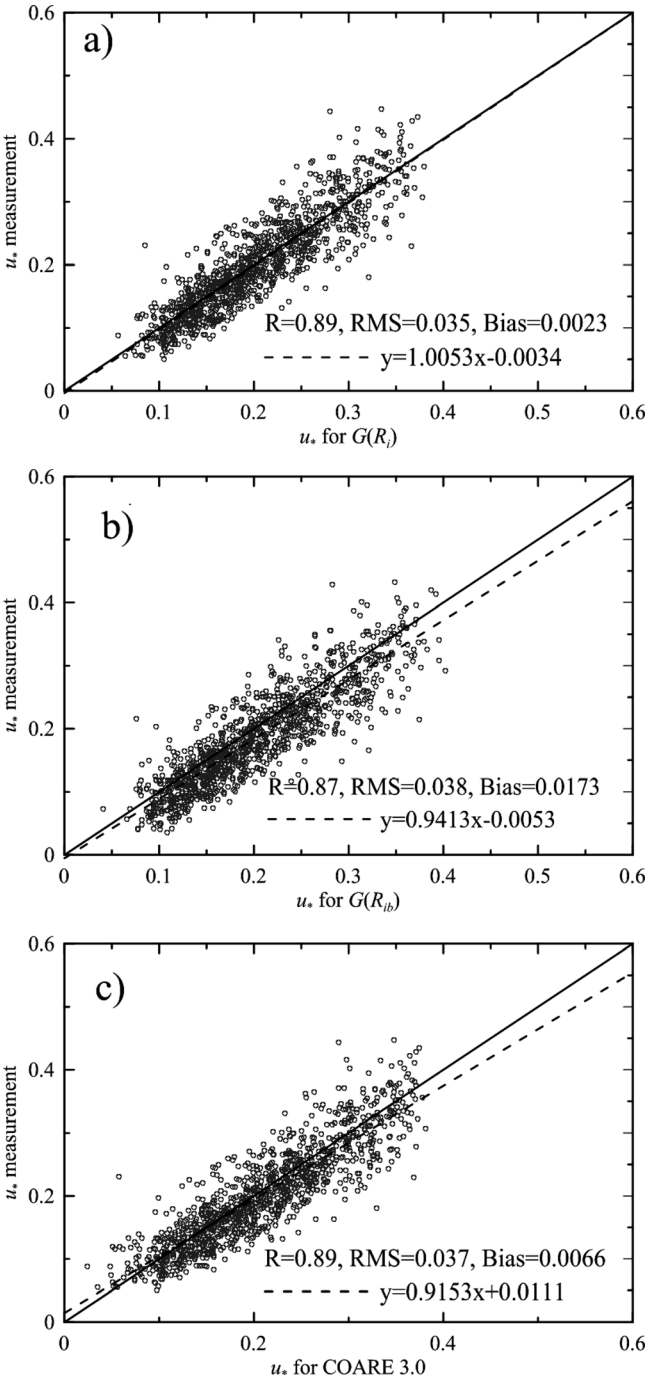

Figure 15. Measured u_* as a function of the friction velocity from (a) R_i, (b) R_{ib}, and (c) COARE 3.0. The solid and dashed lines are 1:1 and best-fit lines, respectively.

$$R_i = 3\times10^4 \frac{\theta_{v*} g z_0}{\theta_0 u_*^2} \tag{31}$$

where it is assumed that $\theta_{v*} = \theta_*(1 + 0.61q_*)$, and the scale coefficient of 3×10^4 is applied to limit the range of R_i between -1.0 and 1.0. According to the Charnock relation, R_i can be further simplified as

$$R_i = 3\times10^4 \alpha \theta_{v*}/\theta_0 \tag{32}$$

where α corresponds to the Charnock constant. R_i is independent of measurement height, and can be easily applied in various situations.

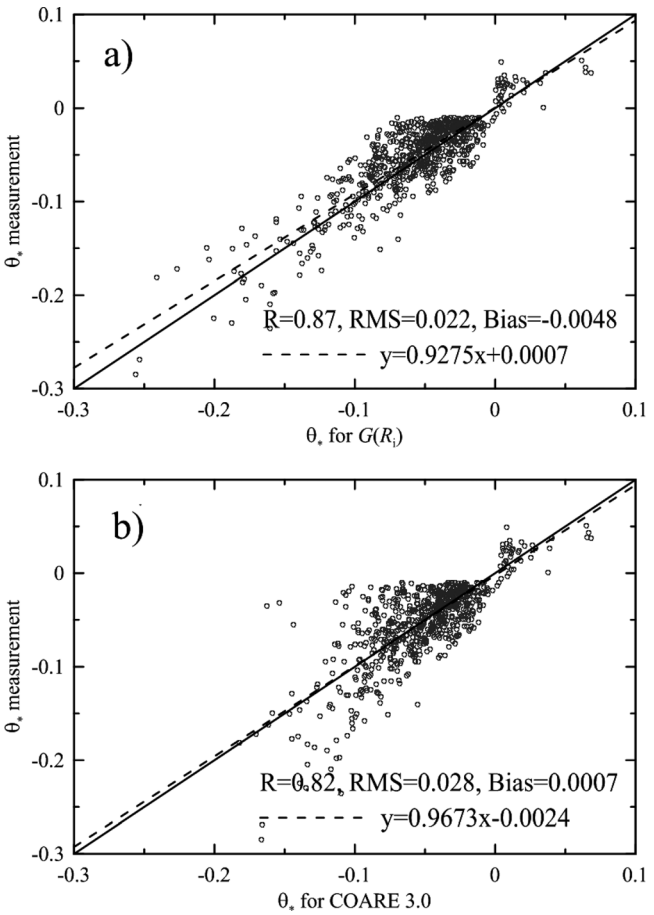

Figure 16. Measured θ_* as a function of θ_* from (a) R_i and (b) COARE 3.0. The solid and dashed lines are 1:1 and best-fit lines, respectively.

We note that considerable efforts have been undertaken to determine the nondimensional gradient as a function of z/L [*Donelan et al.*, 1974]. To compare our work with earlier studies, we checked for relationships between z/L and R_{ib} and R_i. According to their definitions, these relationships can be roughly derived as

$$\frac{z}{L}=R_{ib}\kappa C_H(C_D)^{-3/2} \tag{33}$$

$$\frac{z}{L}=\frac{R_i}{3\times10^4}\kappa\frac{\theta_{v0}}{\theta_v}\exp\left(\kappa/\sqrt{C_{DN}}\right)\approx\frac{R_i}{3\times10^4}\kappa\exp\left(\kappa/\sqrt{C_{DN}}\right) \tag{34}$$

Figure 13 shows a comparison of equations (33) and (34) with our observations. Both equations are quite consistent with the observations.

To derive the stability function G_x versus R_i, we separated the data randomly into two parts: one part was used to derive the new model and it was then tested against the remaining data. From the exchange coefficients and equations (26)–(29), the stability function $G(R_0)$ can be determined. As shown in Figure 14, the results of $G_x(R_i)$ can be fitted as

$$\begin{aligned} G_D(R_i)&=-1.12R_i+1\\ G_H(R_i)&=-2.21R_i+1\\ G_E(R_i)&=-2.63R_i+1 \end{aligned} \tag{35}$$

Figure 15 compares the friction velocities from $G_D(R_i)$, $G_D(R_{ib})$, and COARE 3.0 with the remaining friction velocities. COARE 3.0 was developed for open ocean conditions using a Charnock coefficient that varies with wind speed, whereas the standard Charnock relation has a coefficient tuned to the coastal region

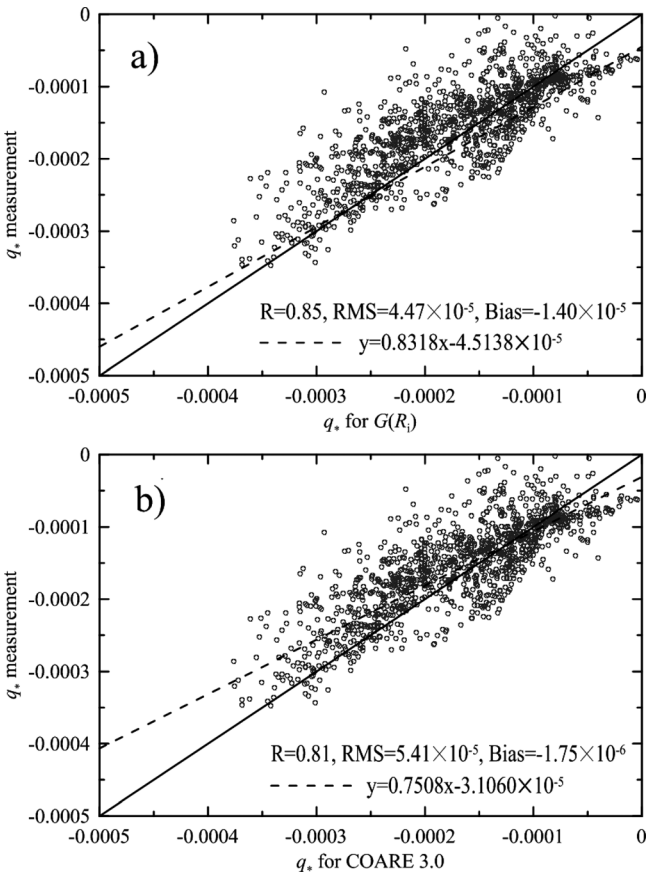

Figure 17. Measured q_* as a function of calculated q_* from (a) R_i and (b) COARE 3.0. The solid and dashed lines are 1:1 and best-fit lines, respectively.

[*Brown et al*., 2013]. In this regard, direct comparison with COARE 3.0 is not possible. In this study, a Charnock coefficient of 1.1×10^{-2} is applied, which is not tuned to the observations.

As shown in Figure 15, it is clear that the performance of R_i is better than that of R_{ib}. The differences in correlation coefficient (R), root mean square (RMS), and bias of the new model and COARE 3.0 against observations are insignificant, which suggests that their differences are small relative to the uncertainty of observations. Figures 16 and 17 show comparisons of measured θ_* and q_* with the new model and with COARE 3.0, respectively. The conclusion can be drawn that the new model is consistent with COARE 3.0 when they are applied to turbulent flux calculations.

8. Conclusion

Based on 2 years of observational data collected during FOPSCS, totals of 12,240, 5813, and 5637 30 min flux runs were used to investigate systematically the behavior of the exchange coefficients for momentum flux, sensible heat flux, and moisture flux, respectively, under low-to-moderate wind conditions. The exchange coefficients were calculated with and without MOST, and were compared to those from previous studies. With MOST, we found that the neutral drag coefficient C_{DN} decreases with wind speed under calm conditions (<5 m/s), then stays nearly constant with wind speed between 5 and 12 m/s, and finally increases at higher wind speeds. This C_{DN} behavior is consistent with previous observational studies. We also found that C_{DN} is greater in offshore wind conditions with short fetch than in onshore winds with long fetch, due to the younger wind waves present in the former case. However, this behavior is not reflected in C_{HN} and C_{EN}. The stability function was also evaluated, and it showed agreement with previous studies. C_{HN} and C_{EN} were found to be independent of wind speed, with values of 1.20 and 0.96, respectively. Relating the friction velocity to the neutral surface wind speed (U_{10N}), we found that they do not exhibit the linear

relationship proposed by *Andreas et al*. [2012] using data from previous field experiments. We fitted a second-order polynomial equation for u_* and U_{10N} using the least squares method and developed a model of C_{DN} as a function of U_{10N}.

Exchange coefficients estimated based on flux data without application of MOST to adjust them to neutral conditions increase with sea-air temperature and humidity differences, but decrease with increased relative humidity. This buoyancy effect can be further described by explicit stability correction, which is a function of the Richardson number. Following *Vickers et al*. [2015], we use a simple model to parameterize u_* as a function of neutral wind speed by fitting the data using the least squares method and multiplying them by a stability function that depends on the Richardson number. In addition to the stability function tested by *Vickers et al*. [2015] as a function of the bulk Richardson number, we introduced a simplified Richardson number that is independent of height and is a function of the Charnock parameter. We derived a new model for exchange coefficients that depends explicitly on stability correction as the simplified Richardson number. We found that the new model performs better than either the traditional bulk Richardson number method or the widely used COARE 3.0 scheme. We note that this is the first study to investigate systematically three exchange coefficients including momentum, heat, and moisture fluxes with and without application of MOST. Our exchange coefficient model can be integrated into coupled atmosphere-ocean models.

Acknowledgments

The authors are grateful to Dianna Francisco for the English proofreading. The efforts of the researchers who obtained and published the data used in this study as well as their funding organizations are greatly appreciated. The observational data gathered from published papers are available from Dongliang Zhao through e-mail: dlzhao@ouc.edu.cn. This work was financially supported by the Public Science and Technology Research Funds Projects of Ocean (201505007), the National Natural Science Foundation of China (NSFC) (41276015), the Joint Project for the National Oceanographic Center by the NSFC and Shandong Government (U1406401), and the Doctoral Fund of the Ministry of Education of China (20120132110004).

References

Andreas, E. L., L. Mahrt, and D. Vickers (2012), A new drag relation for aerodynamically rough flow over the ocean, *J. Atmos. Sci.*, *69*(8), 2520–2537, doi:10.1175/JAS-D-11-0312.1.

Baas, P., B. J. H. van de Wiel, and A. A. M. Holtslag (2006), Exploring self-correlation in flux-gradient relationships for stably stratified conditions, *J. Atmos. Sci.*, *63*(11), 3045–3054, doi:10.1175/JAS3778.1.

Banner, M. L., W. Chen, E. J. Walsh, J. B. Jensen, S. Lee, and C. Fandry (1999), The Southern Ocean waves experiment. Part I: Overview and mean results, *J. Phys. Oceanogr.*, *29*(9), 2130–2145, doi:10.1175/1520-0485(1999)029 < 2130:TSOWEP>2.0.CO;2.

Bianco, L., J. W. Bao, C. W. Fairall, and S. A. Michelson (2011), Impact of sea-spray on the atmospheric surface layer, *Boundary Layer Meteorol.*, *140*(3), 361–381, doi:10.1007/s10546-011-9617-1.

Bradley, E. F., P. A. Coppin, and J. S. Godfrey (1991), Measurements of sensible and latent heat flux in the western equatorial Pacific Ocean, *J. Geophy. Res.*, *96*, 3375–3389, doi:10.1029/90JC01933.

Brown, J. M., L. O. Amoudry, F. M. Mercier, and A. J. Souza (2013), Intercomparison of the Charnock and COARE bulk wind stress formulations for coastal ocean modeling, *Ocean Sci.*, *9*(4), 721–729, doi:10.5194/os-9-721-2013.

Bumke, K., M. Schlundt, J. Kalisch, A. Macke, and H. Kleta (2014), Measured and parameterized energy fluxes estimated for Atlantic transects of R/V Polarstern, *J. Phys. Oceanogr.*, *44*(2), 482–491, doi:10.1175/JPO-D-13-0152.1.

Businger, J. A., J. C. Wyngaard, Y. Izumi, and E. F. Bradley (1971), Flux-profile relationships in the atmospheric surface layer, *J. Atmos. Sci.*, *28*(2), 181–189, doi:10.1175/1520-0469(1971)028 < 0181:FPRITA>2.0.CO;2.

Charnock, H. (1955), Wind stress on a water surface, *Q. J. R. Meteorol. Soc.*, *81*(350), 639–640, doi:10.1002/qj.49708135027.

Cook, P. A., and I. A. Renfrew (2015), Aircraft-based observations of air-sea turbulent fluxes around the British Isles, *Q. J. R. Meteorol. Soc.*, *141*(686), 139–152, doi:10.1002/qj.2345.

DeCosmo, J., K. B. Katsaros, S. D. Smith, R. J. Anderson, W. A. Oost, K. Bumke, and H. Chadwick (1996), Air-sea exchange of water vapor and sensible heat: The humidity exchange over the sea (HEXOS) results, *J. Geophy. Res. Oceans*, *101*, 12,001–12,016, doi:10.1029/95JC03796.

Donelan, M. A., K. N. Birch and D. C. Beesley (1974), Generalized Profiles of Wind Speed, Temperature and Humidity, in *Proceedings of the 17th Conference on Great Lakes Research*, International Association of Great Lakes Research, pp. 369–388, Ann Arbor, Mich. [Available at http://iaglr.org/conference/past.php.]

Donelan, M. A., B. K. Haus, N. Reul, W. J. Plant, M. Stiassnie, H. C. Graber, O. B. Brown, and E. S. Saltzman (2004), On the limiting aerodynamic roughness of the ocean in very strong winds, *Geophys. Res. Lett.*, *31*, L18306, doi:10.1029/2004GL019460.

Drennan, W. M., H. C. Graber, D. Hauser, and C. Quentin (2003), On the wave age dependence of wind stress over pure wind seas, *J. Geophy. Res.*, *108*(C3), 8062, doi:10.1029/2000JC000715.

Drennan, W. M., J. A. Zhang, J. R. French, C. McCormick, and P. G. Black (2007), Turbulent fluxes in the hurricane boundary layer: Part II: Latent heat flux, *J. Atmos. Sci.*, *64*(4), 1103–1115, doi:10.1175/JAS3889.1.

Edson, J., et al. (2007), The coupled boundary layers and air-sea transfer experiment in low winds, *Bull. Am. Meteorol. Soc.*, *88*, 341–356.

Edson, J., V. Jampana, R. A. Weller, S. P. Bigorre, A. J. Plueddemann, C. W. Fairall, S. D. Miller, L. Mahrt, D. Vickers, and H. Hersbach (2013), On the exchange of momentum over the open ocean, *J. Phys. Oceanogr.*, *43*(8), 1589–1610, doi:10.1175/JPO-D-12-0173.1.

Fairall, C. W., E. F. Bradley, D. P. Rogers, J. B. Edson, and G. S. Young (1996), Bulk parameterization of air-sea fluxes for tropical ocean-global atmosphere coupled-ocean atmosphere response experiment, *J. Geophy. Res.*, *101*, 3747–3764, doi:10.1029/95JC03205.

Fairall, C. W., E. F. Bradley, J. E. Hare, A. A. Grachev, and J. B. Edson (2003), Bulk parameterization of air-sea fluxes: Updates and verification for the COARE algorithm, *J. Clim.*, *16*(4), 571–591, doi:10.1175/1520-0442(2003)016 < 0571:BPOASF>2.0.CO;2.

Foreman, R. J., and S. Emeis (2010), Revisiting the definition of the drag coefficient in the marine atmospheric boundary layer, *J. Phys. Oceanogr.*, *40*(10), 2325–2332, doi:10.1175/2010JPO4420.1.

Frederickson, P. A., and K. L. Davidson (2003), Observational buoy studies of coastal air-sea fluxes, *J. Clim.*, *16*(4), 593–599, doi:10.1175/1520-0442(2003)016 < 0593:OBSOCA>2.0.CO;2.

French, J. R., W. M. Drennan, J. A. Zhang, and P. G. Black (2007), Turbulent fluxes in the hurricane boundary layer: Part I: Momentum flux, *J. Atmos. Sci.*, *64*(4), 1089–1102, doi:10.1175/JAS3887.1.

Garratt, J. R. (1977), Review of drag coefficients over oceans and continents, *Mon. Weather Rev.*, *105*(7), 915–929, doi:10.1175/1520-0493(1977105 < 0915:RODCOO>2.0.CO;2.

Garrat, J. R. (1992), *The Atmospheric Boundary Layer*, 316 pp., Cambridge Univ. Press, Cambridge, U. K.

Geernaert, G. L., K. B Katsaros, and K. Richter (1986), Variation of the drag coefficient and its dependence on sea state, *J. Phys. Oceanogr.*, *91*(C6), 7667–7679, doi:10.1029/JC091iC06p07667.
Grachev, A. A., and C. W. Fairall (2001), Upward momentum transfer in the marine boundary layer, *J. Phys. Oceanogr.*, *31*(7), 1698–1711, doi:10.1175/1520-0485(2001031 < 1698:UMTITM>2.0.CO;2.
Hicks, B. B. (1978), Some limitations of dimensional analysis and power laws, *Boundary Layer Meteorol.*, *14*(4), 567–569, doi:10.1007/BF00121895.
Högström, U. L. F. (1988), Non-dimensional wind and temperature profiles in the atmospheric surface layer: A re-evaluation: Topics in Micrometeorology, *Boundary Layer Meteorol.*, *42*, 55–78, doi:10.1007/978-94-009-2935-7_6.
Högström, U. L. F. (1996), Review of some basic characteristics of the atmospheric surface layer, *Boundary Layer Meteorol.*, *78*, 215–246, doi:10.1007/978-94-017-0944-6_11.
Holthuijsen, L. H., M. D. Powell, and J. D. Pietrzak (2012), Wind and waves in extreme hurricanes, *Geophys. Res. Lett.*, *117*, C09003, doi:10.1029/2012JC007983.
Jarosz, E., D. A. Mitchell, D. W. Wang, and W. J. Teague (2007), Bottom-up determination of air-sea momentum exchange under a major tropical cyclone, *Science*, *315*(5819), 1707–1709, doi:10.1126/science.1136466.
Kara, A. B., H. E. Hurlburt, and A. J. Wallcraft (2005), Stability-dependent exchange coefficients for air-sea fluxes, *J. Atmos. Oceanic Technol.*, *22*(7), 1080–1094, doi:10.1175/JTECH1747.1.
Klipp, C. L., and L. Mahrt (2004), Flux-gradient relationship, self-correlation and intermittency in the stable boundary layer, *Q. J. R. Meteorol. Soc.*, *130*(601), 2087–2103, doi:10.1256/qj.03.161.
Large, W. G. and S. Pond (1981), Open ocean momentum flux measurements in moderate to strong winds, *J. Phys. Oceanogr.*, *11*(3), 324–336, doi:10.1175/1520-0485(1981)011 < 0324:OOMFMI>2.0.CO;2.
Large, W. G., and S. Pond (1982), Sensible and latent heat flux measurements over the ocean. *J. Phys. Oceanogr.*, *12*(5), 464–482, doi:10.1175/1520-0485(1982)012 < 0464:SALHFM>2.0.CO;2.
Liu, W. T., K. B. Karsaros, and J. A. Businger (1979), Bulk parameterization of air-sea exchange of heat and water vapor including the molecular constraints at the interface, *J. Atmos. Sci.*, *36*, 1722–1735, doi:10.1175/1520-0469(1979)036 < 1722:BPOASE>2.0.CO;2.
Mahrt, L., D. Vickers, J. Howell, J. Hojstrup, J. M. Wilczak, J. Edson, and J. Hare (1996), Sea surface drag coefficients in the Risø Air Sea Experiment, *J. Geophy. Res.*, *101*, 14,327–14,335, doi:10.1029/96JC00748.
Mahrt, L., D. Vickers, J. Sun, N. O. Jensen, H. Jørgensen, E. Pardyjak, and H. Fernando (2001), Determination of the surface drag coefficient, *Boundary Layer Meteorol.*, *99*(2), 249–276, doi:10.1023/A:1018915228170.
McGillis, W. R., et al. (2004), Air-sea CO_2 exchange in the equatorial Pacific, *J. Geophy. Res.*, *109*, C08S02, doi:10.1029/2003JC002256.
McMillen, R. T. (1988), An eddy correlation technique with extended applicability to non-simple terrain, *Boundary Layer Meteorol.*, *43*(3), 231–245, doi:10.1007/BF00128405.
Monin, A. S. and A. M. Yaglom (1971), *Statistical Fluid Mechanics*, vol. 1, 769 pp., MIT Press, Cambridge, Mass.
Oncley, S. P., C. A. Friehe, J. C. Larue, J. A. Businger, E. C. Itsweire, and S. S. Chang (1996), Surface-layer fluxes, profiles, and turbulence measurements over uniform terrain under near-neutral conditions, *J. Atmos. Sci.*, *53*(7), 1029–1044, doi:10.1175/1520-0469(1996)053 < 1029:SLFPAT>2.0.CO;2.
Pond, S., G. T. Phelps, J. E. Paquin, G. McBean, and R. W. Stewart (1971), Measurements of the turbulent fluxes of momentum, moisture and sensible heat over the ocean, *J. Atmos. Sci.*, *28*(6), 901–917, doi:10.1175/1520-0469(1971)028 < 0901:MOTTFO>2.0.CO;2.
Persson, G., P. Ola, J. E. Hare, C. W. Fairall, and W. D. Otto (2005), Air-sea interaction processes in warm and cold sectors of extratropical cyclonic storms observed during FASTEX, *Q. J. R. Meteorol. Soc.*, *131*(607), 877–912, doi:10.1256/qj.03.181.
Petersen, G. N., and I. A. Renfrew (2009), Aircraft-based observations of air-sea fluxes over Denmark Strait and the Irminger Sea during high wind speed conditions, *Q. J. R. Meteorol. Soc.*, *135*(645), 2030–2045, doi:10.1002/qj.355.
Powell, M. D., P. J. Vickery, and T. A. Reinhold (2003), Reduced drag coefficient for high wind speeds in tropical cyclones, *Nature*, *422*(6929), 279–283, doi:10.1038/nature01481.
Smith, S. D. (1980), Wind stress and heat flux over the ocean in gale force wind, *J. Phys. Oceanogr.*, *10*(5), 709–726, doi:10.1175/1520-0485(1980)010 < 0709:WSAHFO>2.0.CO;2.
Smith, S. D. (1989), Water vapor flux at the sea surface, *Boundary Layer Meteor.*, *47*(1–4), 277–293, doi:10.1007/BF00122334.
Smith, S. D., et al. (1992), Sea surface wind stress and drag coefficients: The HEXOS results, *Boundary Layer Meteorol.*, *60*(1–2), 109–142, doi:10.1007/BF00122064.
Sun, J., D. Vandemark, L. Mahrt, D. Vickers, T. Crawford, and C. Vogel (2001), Momentum transfer over the coastal zone, *J. Geophy. Res.*, *106*, 12,437–12,448, doi:10.1029/2000JD900696.
Tanner, C. B., and G. W. Thurtell (1969), Anemoclinometer measurements of Reynolds stress and heat transport in the atmospheric surface layer, *Tech. Rep. ECOM-66-G22-F*, 82 pp, Univ. of Wisconsin, Madison, Wis.
Toffoli, A., L. Loffredo, P. Le Roy, J. M. Lefèvre, and A. V. Babanin (2012), On the variability of sea drag in finite water depth, *J. Geophy. Res.*, *117*, C00J25, doi:10.1029/2011JC007857.
Vickers, D., and L. Mahrt (1997), Quality control and flux sampling problems for tower and aircraft data, *J. Atmos. Oceanic Technol.*, *14*(3), 512–526, doi:10.1175/1520-0426(1997)014 < 0512:QCAFSP>2.0.CO;2.
Vickers, D., and L. Mahrt (2006), A solution for flux contamination by mesoscale motions with very weak turbulence, *Boundary Layer Meteorol.*, *118*(3), 431–447, doi:10.1007/s10546-005-9003-y.
Vickers, D., L. Mahrt, and E. L. Andreas (2013), Estimates of the 10-m neutral sea surface drag coefficient from aircraft eddy-covariance measurements, *J. Phys. Oceanogr.*, *43*(2), 301–310, doi:10.1175/JPO-D-12-0101.1.
Vickers, D., L. Mahrt, and E. L. Andreas (2015), Formulation of the sea surface friction velocity in terms of the mean wind and bulk stability, *J. Appl. Meteorol. Climatol.*, *54*(3), 691–703, doi:10.1175/JAMC-D-14-0099.1.
Wilczak, J. M., S. P. Oncley, and S. A. Stage (2001), Sonic anemometer tilt correction algorithms, *Boundary Layer Meteorol.*, *99*(1), 127–150, doi:10.1023/A:1018966204465.
Wu, J. (1980), Wind-stress coefficients over sea surface near neutral conditions-A revisit, *J. Phys. Oceanogr.*, *10*(5), 727–740, doi:10.1175/1520-0485(1980)010 < 0727:WSCOSS>2.0.CO;2.
Yelland, M., and P. K. Taylor (1996), Wind stress measurements from the open ocean, *J. Phys. Oceanogr.*, *26*(4), 541–558, doi:10.1175/1520-0485(1996)026 < 0541:WSMFTO>2.0.CO;2.
Zhang, J. A., P. G. Black, J. R. French, and W. M. Drennan (2008), First direct measurements of enthalpy flux in the hurricane boundary layer: The CBLAST results, *Geophys. Res. Lett.*, *35*, L14813, doi:10.1029/2008GL034374.